Proceedings of Global Power and Propulsion Society
ISSN-Nr: 2504-4400
GPPS Xi'an21
18th–20th October, 2021

www.gpps.global

GPPS-TC-2021-0337

SENSITIVITY OF COMPRESSOR PERFORMANCE AND TIP-LEAKAGE VORTICES TO INHOMOGENEOUS CASING HEAT-FLUX DISTRIBUTIONS

Dajan Mimic*, Philipp Sauer, Joerg R. Seume
Institute of Turbomachinery and Fluid Dynamics
Leibniz Universität Hannover
* mimic@tfd.uni-hannover.de
Garbsen, Germany
Cluster of Excellence SE^{2}A – Sustainable and Energy Efficient Aviation
Technische Universität Braunschweig
Braunschweig, Germany

ABSTRACT

Compressor cooling is a promising method for increasing the efficiency of aero engines. This paper shows that the application of this method is not limited to the thermodynamic effect of extracting the net heat flow, but also extends to the heat-flux distribution provided by the cooling. To demonstrate this, we conducted an extensive numerical study featuring a wide range of heating and cooling distributions applied to the casing of a compressor rotor in a single-stage model, which was taken from the last stage of an experimentally validated four-stage high-speed compressor model. The results show that the benefit – or detriment – of these variations may be significantly impacted by the heat-flux distribution applied. We show that, while the net heat flux proves to be the dominant factor, the local distribution may account for up to 14% in the mass-flow variability and up to 21% of the variation in the adiabatic rotor efficiency. The results suggest an influence of the heat-flux distribution on the tip-leakage vortex.

INTRODUCTION

This paper presents an analysis of the sensitivity of compressor performance and tip-leakage formation to the application of heat-flux distributions on a rotor casing. We show that not only the net heat extraction or input affect the compressor efficiency as can be seen from the definition of entropy, i.e.,

$$\mathrm{d}S = \frac{\delta Q}{T}, \tag{1}$$

but also the distribution of these heat fluxes. An extensive sampling of numerical simulations with different heat-flux distributions imposed onto the casing of a compressor rotor demonstrates that variations in the adiabatic efficiency can be achieved, beyond what is expected from the integrated heat flow. As the cooling of axial compressors presents a promising approach to developing more efficient aero engines, the judicious application of said cooling becomes important. In fact, this paper shows that a disadvantageous application of cooling can act to the detriment of the compressor by lowering its efficiency. The results suggest a link between the thermal effects and changes in the tip-leakage vortex formation.

Cooling in Axial Compressors

The effect of cooling on axial compressors has been discussed by Shah and Tan (2007). In a series of numerical studies conducted on NASA Rotor 37, as well as an eight-stage axial compressor model, the authors demonstrated a great potential for performance increases due to heat extraction. Willeke et al. (2017) obtained similar results in a numerical study of a three-stage axial compressor. However, they estimated the increase in engine weight to be approximately 0.3% for a cooled single-stage compressor and 0.12% for each additional change. This highlights the necessity of a judicious approach towards cooling in aero engines.

Impact on Boundary-Layer Development

The effect of heat fluxes between the boundary layer and the adjacent wall are well documented in the literature (e.g., Schlichting and Gersten, 2006). Experiments conducted by Liepmann and Fila (1947) revealed an earlier transition onset for a boundary-layer of an air flow along a heated flat plate, compared to an unheated plate. According to their analysis, the temperature increase in the near-wall region causes a wall-normal decrease in viscosity which, in turn, promotes the formation of an inflection point in the velocity profile.

This effect was investigated by Cebeci and Smith (1968) as a method for non-invasive boundary-layer tripping. The placement of a heating section at the leading edge of an aerofoil did, however, not yield the expected results. In fact, the temperature drop downstream of the heated strip lead to an increased resilience of the boundary layer against transition.

Subsequent studies, using water instead of air, showed – up to a certain point – a stabilisation of the boundary layer when heating was applied (e.g., Wazzan et al., 1967, 1972; Strazisar et al., 1977). Herwig and Schäfer (1992) observed a stabilisation of boundary layers in air and water flows along cooled and heated flat plates, respectively. This seemingly adverse behaviour further cemented the theorised influence of the wall-normal viscosity gradient, as the inverse temperature dependence of the viscosity in gases compared to liquids reconciles the observations for both air and water flows.

Impact on Secondary Flow

Physical mechanisms which affect boundary layers are also likely to affect secondary flow. For example, Liu et al. (2018) numerically predicted a reduced separation bubble and, upon further cooling, a reduced corner vortex in a cooled compressor cascade.

In order to further examine the relationship between thermal effects and secondary flow, Mimic et al. (2019) applied various heat-flux distributions to the end wall of a 90° bent duct in a numerical study. The distributions comprised heating and cooling patches in loose analogy to the crests and troughs of end-wall contouring. Beside the expected net heat flow through the domain boundary, the distributions exhibited – even for constant net heat flow – a considerable impact on the loss generation in the duct. Roughly 25% of the viscous dissipation of kinetic energy could be attributed to the distribution, providing an improvement in the dynamic-pressure coefficient of 4.9% for a vanishing net heat flow. The changes were also evident in the boundary-layer momentum thickness and the streamwise vorticity.

The malleability of both boundary layers and secondary-flow vortices in the face of thermal gradients is not only a consequence of the interaction of boundary layers and secondary flow, but also a result of their rotational nature. The behaviour of rotational flows may be described using the vorticity equation:

$$\frac{\mathrm{D}\boldsymbol{\Omega}}{\mathrm{D}t} = \rho\left(\mathbf{u}\otimes\boldsymbol{\nabla}\right)\cdot\boldsymbol{\Omega} - \rho\boldsymbol{\Omega}\left(\boldsymbol{\nabla}\cdot\mathbf{u}\right) + \mu\boldsymbol{\nabla}^2\boldsymbol{\Omega} + \frac{1}{\rho}\boldsymbol{\nabla}\rho\times\boldsymbol{\nabla}p + \boldsymbol{\nabla}\mu\times\left(\boldsymbol{\nabla}^2\mathbf{u}\right) + \rho\frac{1}{3}\boldsymbol{\nabla}\mu\times\left[\boldsymbol{\nabla}(\boldsymbol{\nabla}\cdot\mathbf{u})\right] + \rho\boldsymbol{\nabla}\times\mathbf{f}. \tag{2}$$

The four relevant terms with respect to thermal effects appear in the second line of Eqn. (2). They express the respective contributions of baroclinic density gradients, non-uniform viscosity for both incompressible and compressible components of the flow field, and the fictitious forces acting in a rotating reference frame. The last term suggests a stronger effect of wall heat fluxes on the flow in rotating turbomachinery components than in stationary components.

Hypothesis and Approach

Based on these previous investigations, we state the following general hypothesis: *The beneficial effects of compressor cooling documented in the literature are a function of the net heat flow across the compressor boundaries, as well as the local heat-flux distributions applied.* More specifically, we expect an influence of various axial heat flux distributions on the casing of a compressor rotor on the tip-leakage vortex and, thus, the adiabatic efficiency (defined in Eqn. 5).

In order to test this hypothesis, we apply various axial heat-flux distributions to the rotor casing in an axial compressor stage and analyse their impact on integral performance parameters. Based on the performance data, we identify representative cases for a more detailed assessment of the tip-leakage vortex and its changes with respect to the adiabatic reference.

METHODOLOGY

Compressor Test Rig

The four-stage axial high-speed compressor test rig of the Institute of Turbomachinery and Fluid Dynamics at the Leibniz Universität Hannover provides the experimental evidence for the validation of the numerical model used in this work. The compressor comprises a fixed inlet guide vane and four stages with controlled-diffusion aerofoils, followed by an annular diffuser with divergent hub and casing walls. Further details are given in Tab. 1.

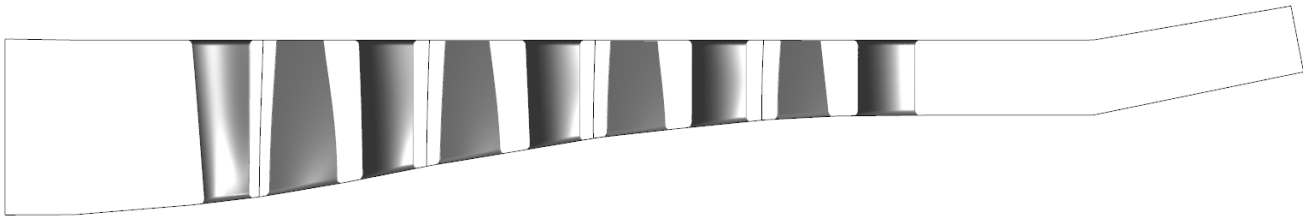

Figure 1 Numerical domain of the four-stage axial compressor

Numerical Model

All simulations were conducted using the turbomachinery flow solver TRACE 9.1.538 developed by the German Aerospace Center (DLR). Turbulence was modelled using the k-ω shear-stress transport (SST) model by Menter et al. (2003), combined with the stagnation-point anomaly fix by Kato and Launder (1993). The γ-Re_θ model in the version presented by Menter et al. (2006) was used to model transition effects. A turbulent Prandtl number of $\mathrm{Pr}_{\mathrm{turb}} = 0.9$ was assumed to compute the heat fluxes. A second-order accuracy finite-volume spatial discretisation was used together with a Fromm scheme and a van Albada-square limiter for the computation of the state variables. The governing equations were solved by incomplete lower-upper (ILU) factorisation.

The structured multi-block mesh of the complete compressor comprises 9.8×10^6 nodes. The results of a mesh convergence are reported in Tab. 2 and preclude a significant grid sensitivity of the numerical results. All boundary layers were resolved by a mesh with a nondimensional wall distance $y^+ < 1$. Mixing planes were used between the rotor and stator domains.

Full-stage validation case

The inlet duct was simulated separately to obtain realistic inlet boundary layers for the full-stage compressor simulations (validation case). In agreement with the experiment, the inlet total pressure was set to 60 kPa at the midspan. The inlet midspan total temperature was set to 288.15 K.

All operating points were simulated at 95% of the design speed. Starting from near-choke conditions, the operating points were set by means of increasing the outlet static pressure until convergence could no longer be achieved. The outlet was then switched to a mass-flow boundary condition; the mass-flow rate was subsequently reduced until convergence could no longer be achieved, which marks the point of numerical surge.

Single-stage test cases

To limit the complexity of the problem at hand, as well as the computation time necessary for the extensive numerical sampling conducted, only the fourth stage of the compressor, including the diffuser, is considered for the numerical test cases. The mesh is taken directly from the full-stage model and consists of 1.8×10^6 cells. Two operating points were simulated: near peak efficiency at 95% of the design speed (PE95) and near numerical surge at 95% of the design speed (NS95). Here, the inlet and outlet boundary conditions were set as the total and static pressure, respectively. The inlet distribution and outlet value were obtained from the full-stage simulations at the corresponding locations and for the corresponding operating points. Only the outlet static pressure of NS95 was increased slightly in comparison with the full-stage model. This was done to leverage the greater numerical stability of the single-stage model and to approach the numerical surge limit even closer.

Table 1 Compressor-performance data at the aerodynamic design point (ADP)

Rotor speed	18 000/min
Mass-flow rate	7.93 kg/s
Total-pressure ratio	2.72
Isentropic efficiency	89.13%
Power	952 kW
Inlet total pressure	60 kPa
Flow coefficient (first stage)	0.72
Loading coefficient (first stage)	0.44
Inflow Mach number at tip of Rotor 1	1.005
Circumferential velocity at the blade tips	320 m/s
Reynolds number (Stator 1)	4×10^5

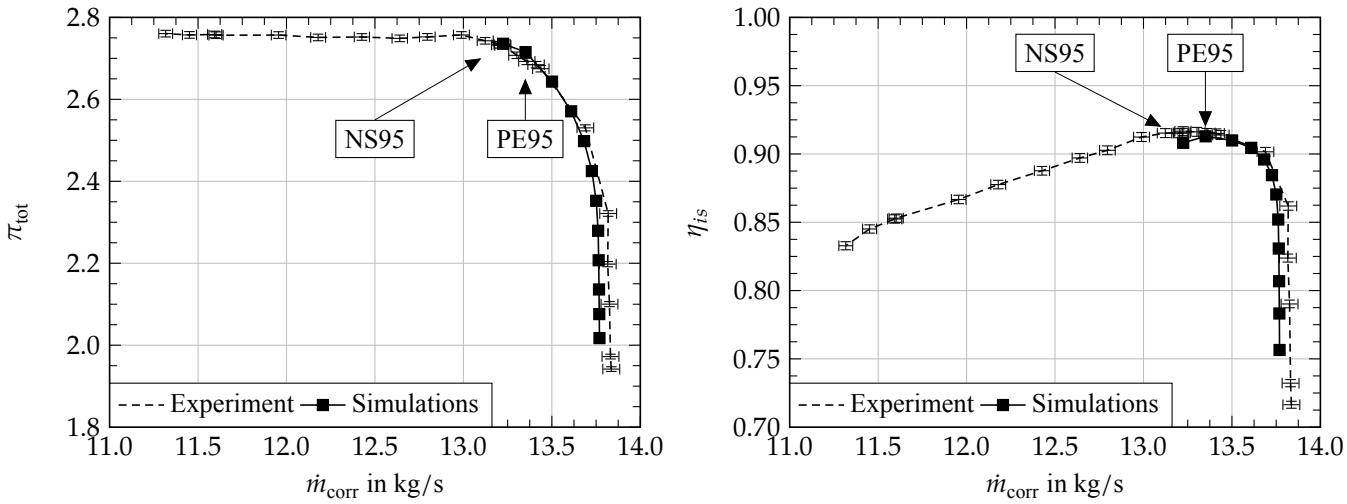

Figure 2 Compressor speed line at 95% of the design speed (experimental data with 95% confidence intervals)

Validation

Figure 2 shows the numerical prediction of the total-pressure ratio and isentropic efficiency for the four-stage compressor against experimental measurements. The comparison shows that the majority of the predicted operating points lies within the 95% confidence intervals. Merely minor deviations can be seen towards the operating limits of the compressor.

Thermal Boundary Condition

The thermal boundary conditions were generated by solving the two-dimensional heat equation on a rectilinear mesh, which represents a circumferential cut through the compressor casing (see Fig. 3). Five heat sources or sinks were positioned equidistantly in the "axial" direction to represent cooling or heating pipes; the number five was chosen to obtain one "pipe" upstream and downstream of the rotor blade as well as three "pipes" along the blade chord. Constant-temperature conditions were assumed at the edges of the domain in order to obtain variable heat-flux distributions as a function of the sources/sinks. The resulting heat fluxes were evaluated at the lower edge of the mesh and mapped as a rotationally symmetric heat-flux boundary condition onto the casing of the numerical compressor model.

Sampling

The heat-flux distributions used in this study were generated by variations of the heat sources/sinks in the heat-equation solver. The samples were generated in three batches for each operating point. The heating or cooling power provided by the individual heat sinks/sources follow normal distributions with a mean value of 0 W and standard deviations of 154 W, 242 W, and 330 W for the respective batches. This batch-wise approach, together with the normal sample distribution, yields a higher sampling density close to the adiabatic reference, i.e., for moderate heat fluxes.

In addition to the adiabatic reference cases, 300 unique heat-flux distributions were sampled for both operating points. Excluding simulation which did not achieve satisfactory convergence, a total of 297 and 287 cases are considered for the near peak-efficiency and near-surge operating points, respectively.

Table 2 Grid-convergence indices

	η_{is}	$\dot{m}$	π_{tot}
ϵ_{21}	0.0147	0.2923	0.0152
ϵ_{32}	0.0004	0.0069	0.0009
ϱ	5.5299	5.4053	4.1408
EERE_{21}	0.0163	0.0382	0.0061
EERE_{32}	0.0004	0.0009	0.0003
GCI_{21}	0.0004	0.001	0.0004
GCI_{32}	7.63×10^{-6}	2.14×10^{-5}	2.07×10^{-5}

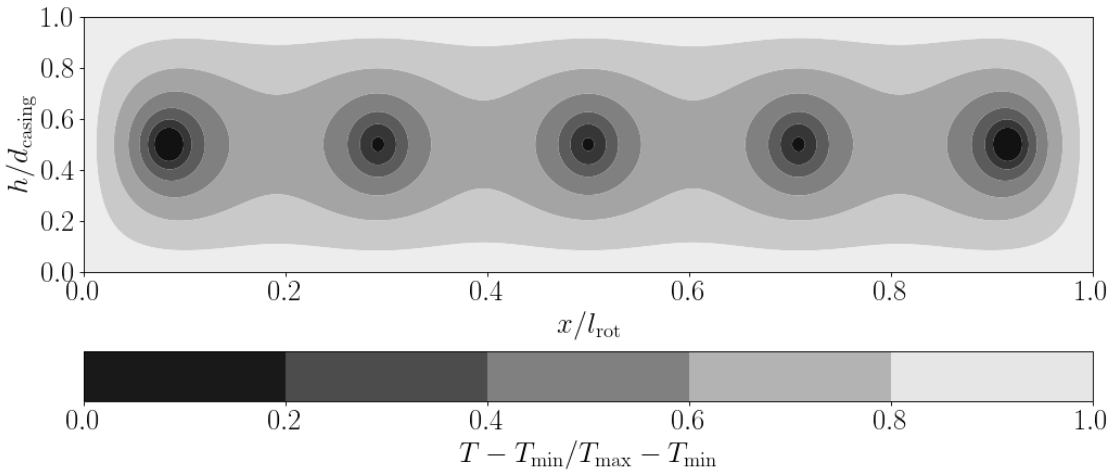

Figure 3 Exemplary temperature distribution (longitudinal section through the rotor casing)

RESULTS AND DISCUSSION

For the following analysis, integral performance parameters of both the stage and the thermally influenced rotor are discussed, as well as the increase in vorticity throughout the rotor domain. All integral parameters are plotted against the non-dimensional heat flow which follows the definition of Shah and Tan (2007) and describes the overall heat flow in relation to the total-enthalpy flow at the stage inlet where $\dot{Q} < 0$ represents cooling:

$$q^+ := \frac{\dot{Q}}{\dot{m} h_{\mathrm{tot,in}}}. \tag{3}$$

Stage

As shown in Fig. 4, the relative mass-flow rate difference, i.e.,

$$\tilde{\Delta}\dot{m} := \frac{\dot{m} - \dot{m}_{\mathrm{ref}}}{\dot{m}_{\mathrm{ref}}}, \tag{4}$$

exhibits the expected increase for net cooling. Interesting for the topic of this paper, however, is the scattering of the data: near peak efficiency (PE95) the distribution causes a variation of approximately 0.07% in the mass-flow rate relative to the adiabatic reference case for constant q^+. This variation increases slightly towards more extreme net heat flows. Expressed in statistical terms, the squared Pearson coefficient is $R^2 \approx 90\%$ for PE95. This means that about 10% of the total variation in the data cannot be explained by the net heat flow, but are a product of the heat-flux distribution. This statistically determined influence of the heat-flux distribution increases to $100\% - R^2 \approx 14\%$ for NS95 and corresponds to a variation of approximately 0.09% in the mass-flow rate relative to the adiabatic reference case for constant q^+. This more pronounced scattering under near-stall conditions is likely a result of both lower mass-flow rates and more pronounced secondary flow, which may amplify the effect of individual heat-flux distributions.

The static and total-pressure ratios of both the stage and the rotor exhibit virtually no sensitivity towards both overall heat flow and heat-flux distribution, the former of which is consistent with the results of Willeke et al. (2017). These results are, therefore, not shown in this paper.

The adiabatic efficiency which is defined according to Shah and Tan (2007), i.e.,

$$\eta_{\mathrm{ad}} := \frac{\pi_{\mathrm{tot}}^{\frac{\gamma-1}{\gamma}} - 1}{\tau_{\mathrm{tot}} - 1 - q^+}, \tag{5}$$

corrects for the reversible entropy changes due to the heat fluxes. Here, it is expressed in term of its difference to the reference in absolute percentage points,

$$\Delta\eta_{\mathrm{ad}} := \eta_{\mathrm{ad}} - \eta_{\mathrm{ad,ref}}, \tag{6}$$

where $\eta_{\mathrm{ad,ref}}$ is equivalent to the isentropic efficiency if the reference case is adiabatic. The results are shown in Fig. 4. While the variation is rather small for PE95 ($100\% - R^2 \approx 5\%$), it reaches about 0.06% for vanishing q^+ under near-surge conditions ($100\% - R^2 \approx 14\%$).

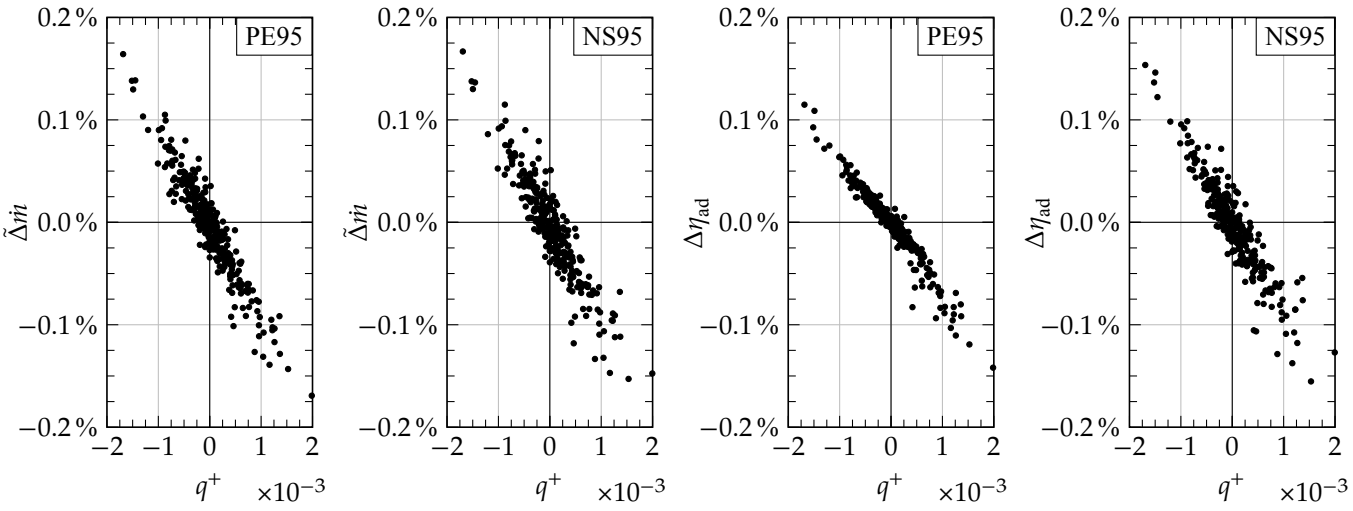

Figure 4 Nondimensional mass-flow rate differences and adiabatic stage efficiencies versus nondimensional mean heat fluxes: near peak efficiency (PE95) and near surge (NS95)

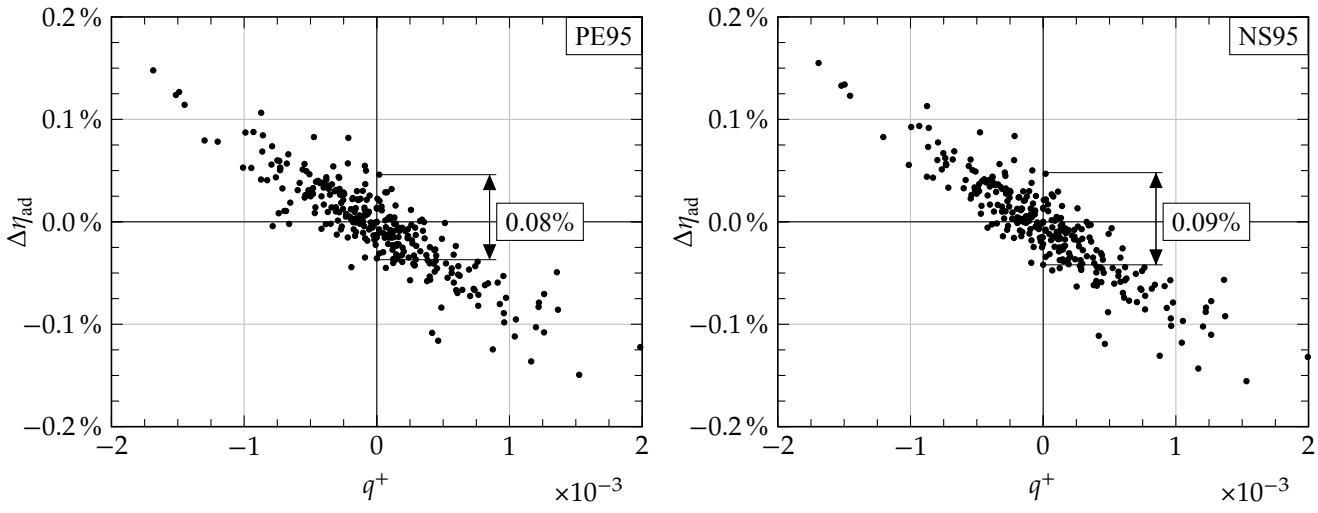

Figure 5 Adiabatic rotor efficiencies versus nondimensional mean heat fluxes: near peak efficiency (PE95) and near surge (NS95)

Rotor

The effects of the heat-flux distributions on the rotor performance – and the tip-leakage vortex in particular – are the central aspect of this paper. As can be seen in Fig. 5, the scattering of the samples is considerably larger than for the stage. This variation, which is induced by the distribution, accounts for $100\% - R^2 \approx 21\%$ of the total variability of the data near peak efficiency and for $100\% - R^2 \approx 17\%$ near the numerical surge. At $q^+ \approx 0$, this corresponds to respective variations in the efficiency of approximately 0.08% and 0.09%.

Tip-leakage vortex

To understand how the different heat-flux distributions affect the tip-leakage vortex, Fig. 6 shows the distribution of the streamwise vorticity on a blade-to-blade cut at 99.5% of the annulus height. Those samples which exhibit the highest and lowest rotor efficiency for a vanishing net heat flow, as well as the reference were selected for this comparison. The heat-flux distributions applied are the same for both operating points.

As denoted in the figure, an improvement in the rotor efficiency is characterised by a reduction in tip-leakage vorticity. The case with an increased efficiency, shown on the right-hand side, exhibits a reduction in the peak streamwise vorticity by about 9% for the operating point PE95, whereas it decreases by approximately 10% for NS95.

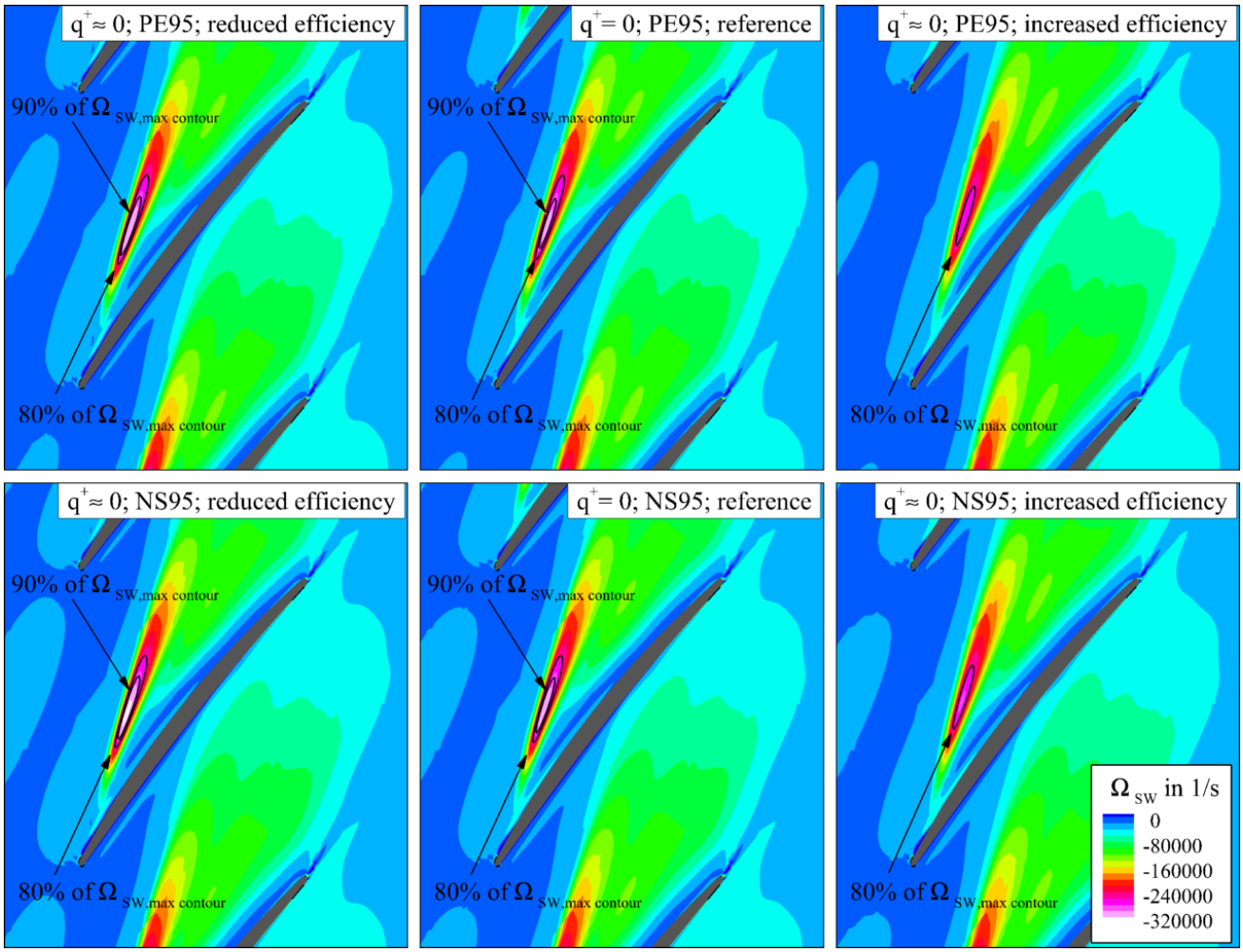

Figure 6 Streamwise vorticity at 99.5% of the annulus height

CONCLUSIONS

As demonstrated in this paper, the local distribution of heat fluxes on the rotor casing in a single compressor stage may account for approximately 10% in the mass-flow variability and circa 21% of the variation in the adiabatic rotor efficiency under peak-efficiency operating conditions, the latter of which represents a variation in the efficiency by about 0.09% at constant net heat flow. Under near-surge conditions, the mass-flow variability due to the distribution increases to circa 14%, whereas the contribution to changes in the efficiency reaches approximately 17%.

For a selection of representative cases at vanishing net heat flow, the results suggest an interaction with the tip-leakage vortex: an advantageous heat-flux distribution decreases the peak streamwise vorticity by roughly 9% at peak efficiency and about 10% near surge.

Further studies on this subject should aim at identifying the dominant changes in the individual entropy-producing mechanisms, which contribute to the observed behaviour. This entails a thorough understanding of how individual heat sources or sinks affect the local flow topology, as well as their mutual interaction.

NOMENCLATURE

Latin Symbols

d	thickness
e	relative error
$\mathbf{f}$	volume-specific force vector
F_S	factor of safety
h	height
h	specific enthalpy
l	length
$\mathbf{n}$	normal vector
$\dot{m}$	mass-flow rate
p	pressure
Pr	Prandtl number
q, q^+	heat flux, nondimensional heat flux
$\dot{Q}$	rate of heat flow
R^2	squared Pearson coefficient
S	duct cross-sectional area
S	entropy
T	temperature
$\mathbf{u}$	velocity vector
y^+	nondimensional wall distance
x	axial direction

Greek Symbols

η	efficiency
ν	kinematic viscosity
π	pressure ratio
ρ	density
ϱ	observed order of accuracy
τ	temperature ratio
$\mathbf{\Omega}$, Ω	vorticity vector, vorticity

Subscripts

ad	corrected
corr	corrected
in	inlet
is	isentropic
max	maximum
min	minimum
ref	reference
rev	reversible
rot	rotor
out	outlet ´
tot	total quantity
turb	turbulent

Acronyms

ADP	cross-passage flow
EERE	estimated extrapolated relative error
GCI	grid convergence index
PE95	operating point near peak efficiency at 95% of the design speed
NS95	operating point near numerical surge at 95% of the design speed

ACKNOWLEDGMENTS

We would like to acknowledge the funding by the Deutsche Forschungsgemeinschaft (DFG, German Research Foundation) under Germany´s Excellence Strategy EXC 2163/1 Sustainable and Energy Efficient Aviation Project ID 390881007. We would also like to acknowledge the contribution of the DLR Institute of Propulsion Technology and MTU Aero Engines AG for providing TRACE. We thank the Leibniz Universität Hannover IT Services (LUIS) for providing computational resources. Furthermore, the authors thank Hye Rim Kim for the fruitful discussions regarding this paper.

REFERENCES

Cebeci, T. and Smith, A. M. O. (1968), 'Investigation of Heat Transfer and of Suction for Tripping Boundary Layers.', *Journal of Aircraft* **5**(5), 450–454.

Herwig, H. and Schäfer, P. (1992), 'Influence of Variable Properties on the Stability of Two-Dimensional Boundary Layers', *Journal of Fluid Mechanics* **243**, 1–14.

Kato, M. and Launder, B. E. (1993), The Modelling of Turbulent Flow Around Stationary and Vibrating Square Cylinders, *in* '9th Symposium on Turbulent Shear Flows', pp. 10.4.1–10.4.6.

Liepmann, H. W. and Fila, G. H. (1947), Investigations of Effects of Surface Temperature and Single Roughness Elements on Boundary-Layer Transition, Report no. 890, National Advisory Committee for Aeronautics.

Liu, L. G., Li, X. S., Ren, X. D. and Gu, C. W. (2018), 'Investigation of Cooling Effect on the Aerodynamic Performance in the Intercooled Compressor', *Journal of Propulsion and Power* **34**(4), 920–932.

Menter, F., Kuntz, M. and Langtry, R. (2003), 'Ten Years of Industrial Experience with the SST Turbulence Model', *Turbulence Heat and Mass Transfer* **4**, 625–632.

Menter, F., Langtry, R., R. Likki, S., Suzen, Y., Huang, P. and Völker, S. (2006), 'A Correlation-Based Transition Model Using Local Variables — Part I: Model Formulation', *ASME J. Turbomach* **128**(3), 413–422.

Mimic, D., Oettinger, M., Jätz, C., Herbst, F. and Seume, J. R. (2019), Thermal End-Wall Contouring, *in* 'Proc. ASME Turbo Expo'. Paper No. GT2019-90191.

Schlichting, H. and Gersten, K. (2006), *Grenzschicht-Theorie*, 10th edn, Springer-Verlag Berlin Heidelberg.

Shah, P. N. and Tan, C. S. (2007), 'Effect of blade passage surface heat extraction on axial compressor performance', *ASME J. Turbomach* **129**(3), 457–467.

Strazisar, A. J., Reshotko, E. and Prahl, J. M. (1977), 'Experimental Study of the Stability of Heated Laminar Boundary Layers in Water', *Journal of Fluid Mechanics* **83**(2), 225–247.

Wazzan, A. R., Keltner, G., Okamura, T. T. and Smith, A. M. O. (1972), 'Spatial Stability of Stagnation Water Boundary Layer with Heat Transfer', *The Physics of Fluids* **15**(12), 2114–2118.

Wazzan, A. R., Okamura, T. T. and Smith, A. M. O. (1967), 'The Stability of Water Flow Over Heated and Cooled Flat Plates', *ASME Journal of Heat Transfer* **90**(1), 109–114.

Willeke, T., Hellberg, M. and Seume, J. R. (2017), A Numerical Concept Study on Internal Blade Cooling in Axial Compressors, *in* 'Proceedings of 12th European Conference on Turbomachinery Fluid dynamics & Thermodynamics'. Paper No. ETC2017-106.